Proceedings of the 2015 International Conference on
Advanced Mechatronic Systems, Beijing, China, August, 22-24, 2015

# Surface Flaws Detection Algorithms for Large Aperture Optical Element

Zhengtao Zhang
Research Center of Precision Sensing and Control, Institute of Automation, Chinese Academy of Sciences
Beijing, China
zhengtao.zhang@ia.ac.cn

Xian tao
Research Center of Precision Sensing and Control, Institute of Automation, Chinese Academy of Sciences
Beijing, China
taoxian2013@ia.ac.cn

De Xu
Research Center of Precision Sensing and Control, Institute of Automation, Chinese Academy of Sciences
Beijing, China
de.xu@ia.ac.cn

Feng Zhang
Research Center of Precision Sensing and Control, Institute of Automation, Chinese Academy of Sciences
Beijing, China
feng.zhang@ia.ac.cn

***Abstract*—In this paper we consider the inspection of surface flaws in large aperture optical element. A high efficiency and precision instrument is proposed which contains two kinds of imaging systems. One is dark-field imaging system (DFIS) constructed by line scan camera with 10μm resolution. The other is bright-field imaging system (BFIS) constructed by microscope with 1μm resolution. Considering the small depth of field of DFIS, an adaptive scanning method based on collimation laser and several focusing points is proposed to keep the clarity of DFIS in large scope scanning. After the scanning, an image mosaic algorithm for the DFIS is presented based on SIFT features and clustering algorithm. Then, the feature extraction algorithm of flaws in DFIS and BFIS is designed. In order to check the flaws more precisely, a location algorithm that can guide the BFIS to inspect the same flaw in DFIS is introduced. Finally, the calibration method of two imaging systems is studied. Experiments show that the device can scan an optical element with size of 810mm×460mm in less than 6min without complex manual operation and the detection precision can reach 3μm satisfying the requirement of practical need.**

***Index Terms*—Large aperture optical element, Image Mosaic, Defect detection, Dark-field imaging system, bright-field imaging system.**

## I. Introduction

At present, precise optical elements are widely used in high power laser systems[1-4], shortwave optics and low-light level imaging and etc.[4-7] However, the flaws on the surface of the optical element may cause damage to the performance of the optical[4]. Different kinds of defects (such as scratches, pitting and etc.) will result in different degrees of laser scattering, energy absorption and diffraction patterns[8, 9].

The automatic inspection of surface imperfections of precise optical elements is a durable problem expected to be solved. Although, more and more scientists focus on the defects detection of the optics and detection method [1, 5, 6, 10-14], there are still many difficulties need to be solved. Such as, how to detect some micro size defects within a large area, the precise calibration method of dark-field bright, image feature extraction algorithm in a complex background, the lighting style and so on.

Nowadays, the majority methods used to detect the flaw are based on the energy scattering of the flaws on the surface of the optics [3, 4, 6, 13, 15-17]. These methods can evaluate the flaws in some extent, but it is difficult to measure the flaws precisely and hard to be calibrated. Some measurement scope can also detect the flaws in detail, but it is not suitable for the large optical element and has very complex data processing[18]. The need of large aperture optical element detection is fast and precise.

In order to track the true damage sites on the surface of an optic, [17] used machine learning tools and data mining techniques to identify and remove signals associated with debris or reflections. [13] designed a rapid feature extraction algorithm based on the combination of vertex chain code and discrete green to improve the extraction speed. A defects detecting method based on Local Area Signal Strength (LASS) and 2-D histogram is theoretically and experimentally proposed in [19]. [20] demonstrates that a machine-learning algorithm can successfully predict the surface location of the damage site using an expanded set of characteristics for each damage site. A digital evaluation system of surface imperfections is proposed in [16, 21, 22]. But this system has to move the heavy optical element in X-Y and it takes 1~2 hours to inspect an optical element with size of 800mm × 400mm.

In this paper, a device is introduced which integrates two kinds of imaging systems. In this way, we can use the advantages of two vision system. As known to all, the dark-field imaging system is difficult to be calibrated precisely especially for small defects. In our device, we can used the

978-1-4673-7996-0/15/$31.00 

DFIS to scan the large aperture optical element within 6min to get the distribution of the flaws with 10μm resolution. Also, we can measure the small flaws using the BFIS in a small scope based on the DFIS image with 1μm resolution. In this way, we can achieve effectiveness and precision at the same time.

The reminder of this paper is organized as follows. Section II introduces the mechanical structure of the equipment and the pose adjustment strategy. In Section III, the image processing and calibration methods of bright-field imaging system are presented in detail. The imaging processing algorithm of dark-field imaging system and calibration method are also discussed in Section IV. Experiments are given to verify the effectiveness of the algorithms in Section V. Finally, the paper is concluded in Section VI.

## II. Instrument Structure Design

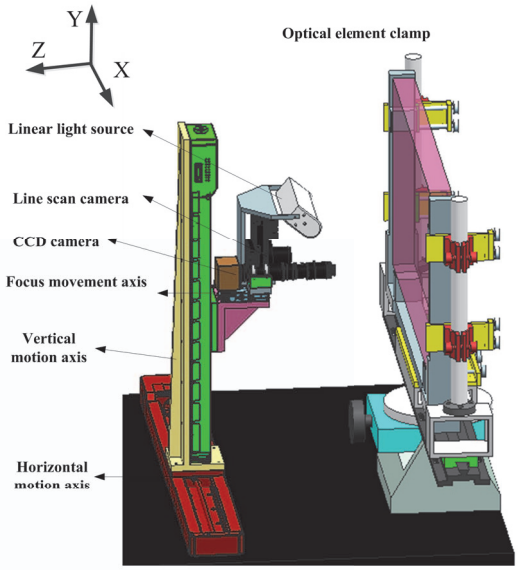


Fig.1 system structure

The main structure of equipment is shown in Fig.1 which contains 3DOF movement axes. The world coordinate is shown in Fig.1 which is coincidence with the motion coordinate. The horizontal motion axis moves along the X direction, the vertical motion axis moves along the Y direction. The line scan camera and CCD camera are armed at the focus movement axis which moves along the Z direction. The line scan camera with the linear light resource constructs the dark-field imaging system with 8K resolution. The CCD camera and microscope lens combined with coaxial light source construct the bright-field imaging system. The optical element clamp has two degree adjust mechanisms which are pitch and yaw. With these angles adjustment design, the surface of the optical element can be vertical to the optical axis of the two cameras.

The depth of the field (DOF) for line scan camera and microscope are 1mm and 40μm, separately. The size of the optical element is with 810mm×460mm. To keep the clarity of the image for line scan camera, the optical axis of the camera should be vertical to the surface of the optical element at first. The function is realized by the optical element clamp using the collimation laser. When the incident light coincides with reflected light, it means that the optical axis of the camera is vertical to the surface of the optical element. The optical axis is paralleled to the collimation laser which are realized by the mechanical installation and calibrated beforehand.

## III. Image Processing of BFIS

### A. adaptive binarization algorithm

In this part, an effective binarization algorithm is designed. First, the gradient of each image coordinate is computed by (1). $(u, v)$ is the image coordinate. $I(u, v)$ is the grey value of the pixel at $(u, v)$. $T(u, v)$ is the maximum gradient value between horizontal and vertical directions.

$$T(u, v) = Max(|I(u+1,v)-I(u-1,v)|,|I(u,v+1)-I(u,v-1)|) \quad (1)$$

Then, $S_T$ denotes the sum of $T(i, j)$ in a small neighbourhood with size $M\times N$. $S_V$ denoting the accumulation of $I(u, v)$ and $T(u, v)$ is also obtained shown in (2). At last, the threshold value of each pixel is computed by $S_T$, $S_V$ and $\delta_T$ where $s$ is an adjustment coefficient. Then the image is binarized by (3) where $I_b(u,v)$ is the grey value of the image after binarization.

$$\begin{cases} S_T = \sum_{u=1}^{M}\sum_{v=1}^{N} T(u,v) \\ S_V = \sum_{u=1}^{M}\sum_{v=1}^{N}\left[I(u,v)*T(u,v)\right] \\ \delta_T = \frac{S_V}{S_T} + s*255 \end{cases} \quad (2)$$

$$I_b(u,v) = \begin{cases} 1, & if\ I(u,v) \geq \delta_T \\ 0, & if\ I(u,v) < \delta_T \end{cases} \quad (3)$$

## IV. Calibration

### A. Calibration of bright-field imaging system

Firstly, the pixel equivalence is calibrated using a calibration gauge. The least space of it is 10μm. So, the pixel equivalence is 0.85μm/pixel.

A Nikon Measurement Microscope is employed to get the true size of chosen flaws. As the Nikon Measurement Microscope is calibrated beforehand, its measurement value can be trusted as true value. 8 flaws are chosen and the measurement values comparison between each other. It can be seen that the two manners coincide with each well and the maximum error is less than 3μm. As the resolution for DFIS is 10μm it can be regard as true value.

### B. Calibration of BFIS

Compared to DFIS, it's much easier to get the actual size of flaws in BFIS, just multiply image size by pixel equivalent.

This can be verified by making use of commercial measuring microscope. A high-precision calibration board can be used to compute the pixel equivalent. On the condition that, the resolution of BFIS is nearly 10 times as much as that of DFIS. The measurement value of flaws in BFIS is regard as true value compared to that measured by DFIS.

## V. Image Capture and Processing of DFIS

The line camera is scanned by column. After the scanning, the sub-images are stitched together to be constructed as a whole image.

According to the principle of DFIS, the image features of flaws are bright and the background is dark. However, the contrast is not sufficient sometimes because of the incident angle of light source and certain type of defects.

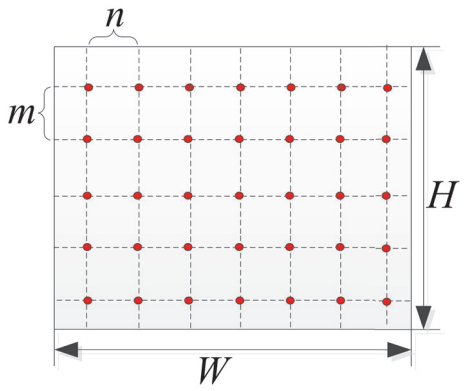


Fig.2 sampled image points

In this section, a binarization algorithm is proposed based on background sampling. First, a series of sampled points are got shown in Fig.2. The sample interval is m row and n column in image space.

$$\begin{cases} T_d = \dfrac{1}{n_1 n_2}\left(\sum_{i=1}^{n_1}\sum_{j=1}^{n_2} I(ni, mj) + \xi_d\right. \\ n_1 = Int(W/n), n_2 = Int(H/m) \end{cases} \tag{4}$$

where $W$ and $H$ are the image width and height respectively, and $I(x, y)$ is the gray value of the pixel in coordinates (x, y). $T_d$ is the threshold and $\xi_d$ is a adjust coefficient.

### A. Calibration of DFIS

The principle of DIFS is introduced as follow. The lighting system usually adopts side lighting way. If there is no flaw on the surface, the background of image is dark. If there are defections located on the surface of the optical element, the object image will be bright on the image plane. However, the relationship between image size and actual size is nonlinear because of the nonlinear scattering effect, especially for small flaws.

To make full advantage of the DFIS and BFIS in our instrument, the flaws can be measured in section. When the flaw size in DFIS is larger than certain value which can be determined by experiment, the relationship between image size and actual size can be fitted by polynomial fit method. Otherwise, it will be measured by the BFIS using the location algorithm given in III. A 3-order polynomial is used as shown in (5) to fit the relationship between image size and actual size in DFIS.

$$L_{ns} = a_0 x^3 + a_1 x^2 + a_2 x^1 + a_3 \tag{5}$$

### B. Chart of Flaw Distribution

The captured image data for a piece of large optical element is huge and over 4G usually. The images even can't be opened in a 32 bit windows OS. However, it is necessary to record the injury state of the optical element in each step, e.g. after the installation, transfer, repairmen and so on. People want to understand the state of the optical element qualitatively in a simple way with fewer amounts of data.

On the other hand, the vast majority of flaws are very small with respect to the entire optical element which means the detected flaws marked on the original image size will be difficult to be observed. At present, inspector marks the substantial distribution of flaws on a A4 paper artificially. This approach is not only inefficient but poor accuracy. Therefore, it is necessary to generate a flaw distribution chart that marks the number and the distribution of flaws in a small image size based on the original detection result of out instrument.

The process of generating chart of flaws distribution (CFD) is based on the binarization method mentioned in section V.B. The flaws' contours in the dark-field images are detected using the freeman chain code. Then, the information of flaws can be obtained which include length, area, contour coordinates and centroid coordinates. The length and area are the most important features of selecting flaws which cared by the inspector. The detected flaws in different size range can be marked with different colors in CFD. In order to make the entire distribution of damage in an appropriate proportion display， the flaws are zoomed with the center of centroid coordinates. The principle of enlarge flaws can be expressed as (6).

$$\begin{cases} u_p' = r_1 \times (u_p - u_{pc}) + r_0 \times u_{pc} \\ v_p' = r_1 \times (v_p - v_{pc}) + r_0 \times v_{pc} \end{cases} \tag{6}$$

where $(u_p, v_p)$ is the pixel coordinates of the point $P$ in a flaw contour in the dark-field images. $(u_{pc}, v_{pc})$ is the centroid coordinates of the flaw contour which include point $P$ in the dark-field images. $(u_p', v_p')$ is the corresponding pixel coordinates of the point $P$ in flaws distribution chart. $r_0$ is a size scale between the flaws distribution chart and the entire dark field image after switching. $r_1$ is the magnification of a single flaw contour.

## VI. Experiments and Results

### A. Experiment System

The practical instrument is shown in Fig.3 (a) which is

described in section II. The vision system of DFIS contains a Dalsa line scan camera and a Schnelder lens with magnification 0.82X shown in Fig.3 (b). The resolution of line scan camera was 8192 pixel and the maximum of line frequency was 68.6 KHz. The pixel equivalence of DFIS is 9.8μm. The depth of field of Schnelder lens is ±0.51mm and the field of view is 70mm. The vision system of BFIS contain a PointGrey CCD camera which equipped with a Navitar zoom lens with magnification 0.47~ 4.5× shown in Fig.3 (b). The capture speed of the camera can reach 15 frames per second with image size of 1280×960 in pixel. The pixel equivalence of DFIS is 1μm. The optical element clamp has two degree adjust mechanisms which are pitch and yaw. The distance of travel of 3DOF motors is 1000mm, 500mm and 50mm for *X*, *Y* and *Z* axis, respectively. The maximum size of the optical element for inspecting is 810×460mm. The CPU of the host computer is Intel Core™2 DUO with frequency of 2.8GHz.

A navigation map is designed to see the HD image easily. The functional part can manage the motion control, image processing of DFIS and BFIS, etc. The detection results of flaws are displayed in result output area line by line.

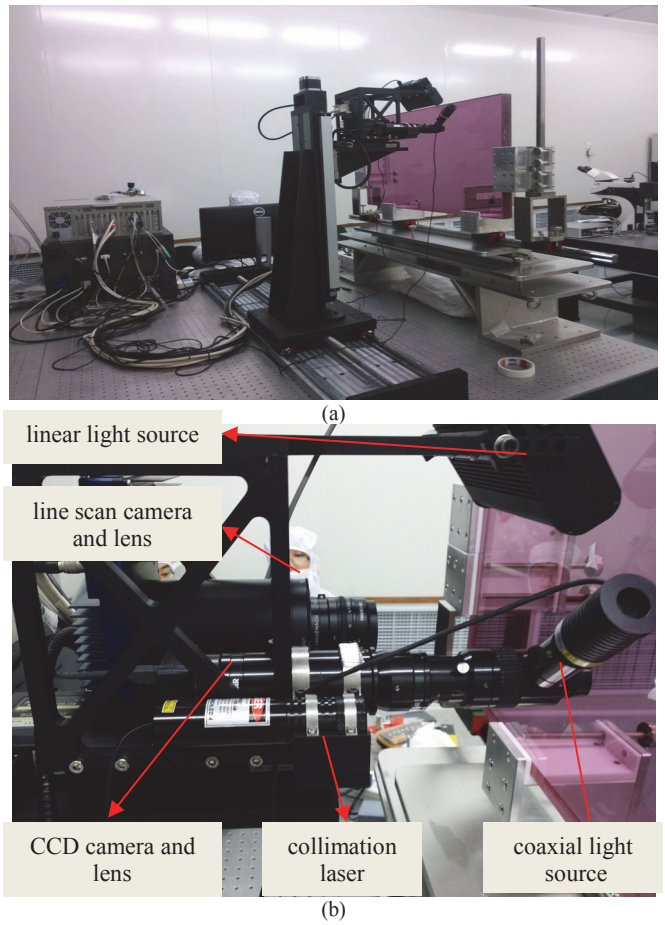


(a)

(b)

Fig.3 Practical device, (a) Practical device, (b) vision part.

## B. *Image processing of DFIS and BFIS*

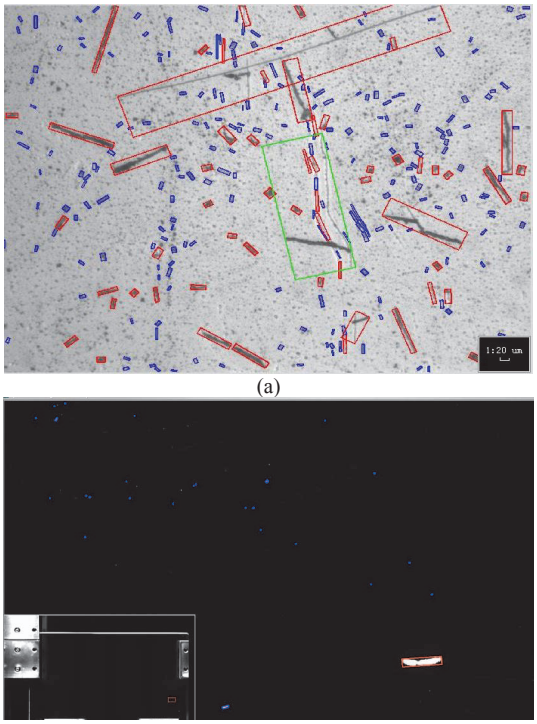

(a)

(b)

Fig.4 Flaws extraction result, (a) flaws in BFIS, (b) flaws in DFIS

The image processing result of BFIS is shown in Fig.4 (a). It can be found that the background of the image is very complex and the grey value of flaws can be dark or bright. The red rectangle denotes the minimum enclosing rectangle of the flaws in image plane. The extraction result of flaws of DFIS is shown in Fig.4 (b). The flaws both in DFIS and DFIS can be detected correctly.

## C. *Calibration of BFIS*

A Nikon Measurement Microscope is employed to get the true size of chosen flaws shown in Fig.5 (a). The according image is shown in Fig.5 (b). As the Nikon Measurement Microscope is calibrated beforehand, its measurement value can be trusted as true value. 8 flaws are chosen and the measurement values comparison between each other is shown in Fig.6. It can be seen that the two manners coincide with each well and the maximum error is less than 3μm. As the resolution for DFIS is 10μm it can be regard as true value.

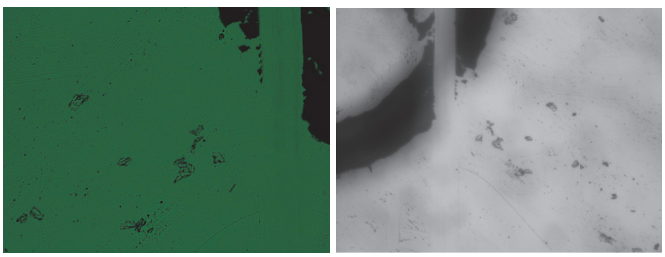

(a) (b)

Fig.5 Flaws image captured by BFIS and Nikon Measurement Microscope (a) captured by Nikon Measurement Microscope, (b) captured by BFIS

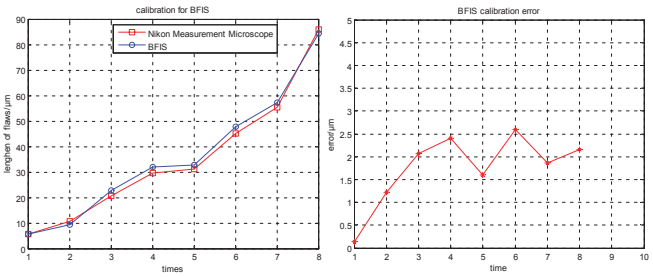


(a) (b)

Fig.6 Calibration result for BFIS, (a) calibration result (b) calibration errors

### *D. Calibration of dark-field imaging system*

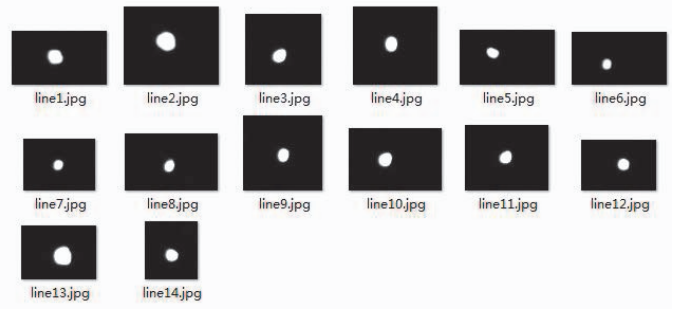


(a) flaws in BFIS

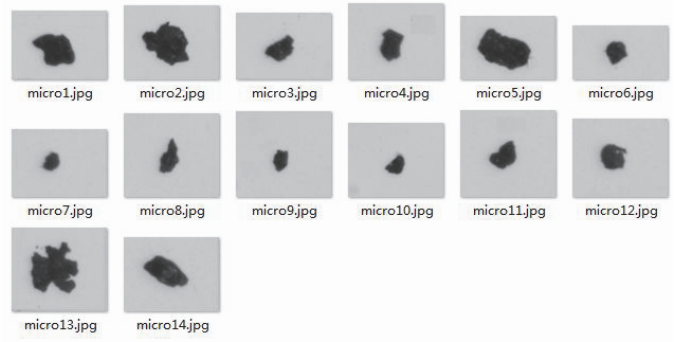


(b) Corresponding flaws in DFIS

Fig.7 images used to calibrate DFIS, (a) flaws in BFIS (b) flaws in DFIS

14 samples of flaws captured by DFIS are given in Fig.7 (a) which sizes are bigger than 50μm. The corresponding flaw images are given in Fig.7 (b). The size of these samples measured by DFIS and BFIS are given in Table I. It can be seen that more details of flaws can be found in BFIS compared to DFIS. Because of the dark-field scattering effect, the image size of flaws in DFIS is larger than actual size shown by Fig.8 (a).

Cubic polynomial is adopted to fit the relationship between the image size in DFIS and the actual size measured by BFIS mentioned in section V.A. The fitting parameters of Fig.7 (b) are shown in (7) is the parameters for Fig.8 (b). Combination Fig.8 (b) and Fig.8(c), we found that the fitting error is less than 3μm when the size of flaw is over 344.4μm.

$$L_{ns} = -0.0001x^3 + 0.0177x^2 + 8.7061x^1 - 20.7394 \quad (7)$$

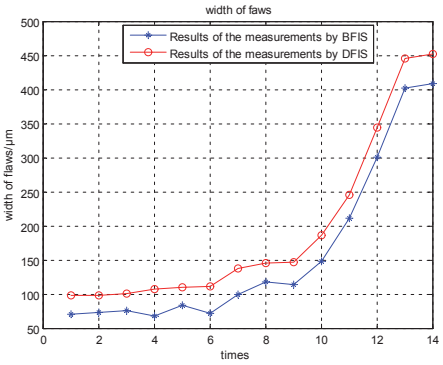


(a)

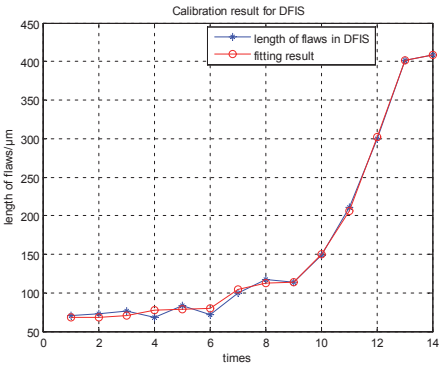


(b)

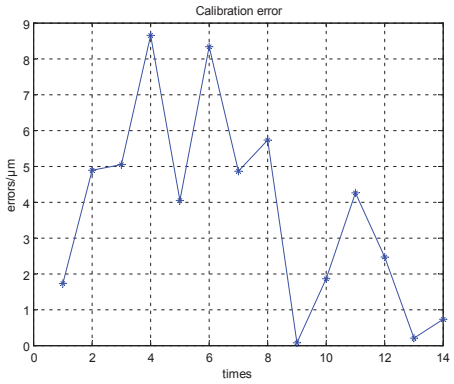


(C)

Fig.8 calibration of big flaws in DFIS, (a) width of flaws measured by DFIS and BFIS, (b) fitting result, (c) calibration error

TABLE I
WIDTH OF BIG FLAWS

| Index | Measured by DFIS/μm | Measured by BFIS/μm |
|---|---|---|
| 1 | 98.2 | 73.1 |
| 2 | 98.2 | 69.9 |
| 3 | 101.2 | 76 |
| 4 | 107.8 | 68.4 |
| 5 | 110.1 | 83.2 |
| 6 | 110.9 | 71.5 |
| 7 | 137.2 | 99.5 |
| 8 | 145.4 | 117.7 |
| 9 | 146.8 | 113.2 |
| 10 | 186.2 | 148.5 |
| 11 | 245.1 | 210.7 |
| 12 | 344.4 | 300 |
| 13 | 445.8 | 401.7 |
| 14 | 452.2 | 409 |

However, the fitting result can't be satisfied when the size of flaws is less than 50μm because of the strong dark-field scattering effect. According to these experimental results 4 important conclusions can be drawn as follows:

- The smaller the flaw size is, the stronger the dark-field scattering effect is.
- When the size of flaw is big enough, a good fitting result can be derived.
- For the smaller flaws, DFIS has bigger amplification effect that is the advantage of DFIS. However, it's difficult to get the actual size by just fitting method.
- An intelligent solution to measure small size of flaws is making good use of BFIS combination with location algorithm based on DFIS.

## VII. CONCLUSION

In this paper, a novelty instrument for large aperture optical element is presented. The device has good adaptation, precision and real-time performance. Without complex manual operation, the device can scan the optical element automatically based on the collimator laser and several focusing points within 6 min. Using the location method based on DFIS image, the BFIS can scan the flaw automatically and more precisely. The calibration results can be used to measure the bigger flaws whose size is over 344 μm in DFIS with fitting of polynomial. The adaptive binarization method of DFIS and BFIS is also introduced. A chart of flaw distribution is generated by the system to give an overall description of the flaws for the optical element. Experiments show that the instrument can meet the needs of efficiency, adaption and precision of inspection for large aperture optical elements.

## ACKNOWLEDGMENT

The authors would like to thank Zhao Xiong, Changchun Liu who are with Laser Fusion Research Center, Chinese Academy of Engineering Physics, Mianyang 621900, P. R. China for their helpful suggestions for our instrument.

## REFERENCES

[1] E. I. Moses, J. H. Campbell, C. J. Stolz, and C. R. Wuest, "The National Ignition Facility: the world's largest optics and laser system," *Optical Engineering at the Lawrence Livermore National Laboratory,* vol. 5001, pp. 1-15, 2003.

[2] J. H. Campbell, R. A. Hawley-Fedder, C. J. Stolz, J. A. Menapace, M. R. Borden, P. K. Whitman*, et al.*, "NIF optical materials and fabrication technologies: an overview," in *Lasers and Applications in Science and Engineering*, 2004, pp. 84-101.

[3] C. E. Thompson, C. F. Knopp, and D. E. Decker, "Optics damage inspection for the NIF," in *Third International Conference on Solid State Lasers for Application to Inertial Confinement Fusion*, 1999, pp. 921-932.

[4] A. Conder, T. Alger, S. Azevedo, J. Chang, S. Glenn, L. Kegelmeyer*, et al.*, "Final optics damage inspection (FODI) for the National Ignition Facility," in *Boulder Damage Symposium XXXIX: Annual Symposium on Optical Materials for High Power Lasers*, 2007, pp. 672010-672010-15.

[5] W. Jun, G. Udupa, and B. Ngoi, "High-speed imaging for evaluation of silicon wafer defects," in *SPIE proceedings series*, 2005.

[6] C. P. Pais, J. A. Silva, J. C. Freitas, F. D. Carvalho, and F. C. Rodrigues, "An Optical-System for the Detection of Surface Imperfections in Ceramics for Use in a Computer-Based Quality-Control Machine," *Optics, Illumination, and Image Sensing for Machine Vision Vi,* vol. 1614, pp. 57-62, 1992.

[7] F. L. Ravizza, M. C. Nostrand, L. M. Kegelmeyer, R. A. Hawley, and M. A. Johnson, "Process for rapid detection of fratricidal defects on optics using linescan phase-differential imaging," in *Laser Damage Symposium XLI: Annual Symposium on Optical Materials for High Power Lasers*, 2009, pp. 75041B-75041B-11.

[8] I. F. Stowers, "Optical cleanliness specifications and cleanliness verification," in *SPIE's International Symposium on Optical Science, Engineering, and Instrumentation*, 1999, pp. 525-530.

[9] G. Bhar, A. Chaudhary, and P. Kumbhakar, "Study of laser induced damage threshold and effect of inclusions in some nonlinear crystals," *Applied surface science,* vol. 161, pp. 155-162, 2000.

[10] J. A. Detrio and S. M. Miner, "Standardized total integrated scatter measurements of optical surfaces," *Optical Engineering,* vol. 24, pp. 243419-243419-, 1985.

[11] T. A. Germer, C. Wolters, and D. Brayton, "Calibration of wafer surface inspection systems using spherical silica nanoparticles," Optics Express, vol. 16, pp. 4698-4705, 2008.

[12] D. Sun, Y. Yang, F. Wang, L. Yang, and R. Li, "Microscopic scattering imaging system of defects on ultra-smooth surface suitable for digital image processing," in Proc. SPIE, 2005, pp. 213-218.

[13] C. Yang, R. Lu, and N. Chen, "A Fast Method for Large Aperture Optical Elements Surface Defects Detection," in Advances in Multimedia, Software Engineering and Computing Vol. 2, ed: Springer, 2012, pp. 175-184.

[14] G. M. Bilmes, D. J. Orzi, O. E. Martinez, and A. Lencina, "New method for real-time surface cleanliness measurement," in Optical Metrology, 2005, pp. 980-986.

[15] S. Wang, Y. Tian, C. J. Tay, and C. Quan, "Development of a laser-scattering-based probe for on-line measurement of surface roughness," Applied optics, vol. 42, pp. 1318-1324, 2003.

[16] F. Q. Wang, Y. Y. Yang, D. D. Sun, L. M. Yang, and R. J. Li, "Digital realization of precision surface defect evaluation system - art. no. 61500F," 2nd International Symposium on Advanced Optical Manufacturing and Testing Technologies: Optical Test and Measurement Technology and Equipment, Pts 1 and 2, vol. 6150, pp. F1500-F1500, 2006.

[17] G. M. Abdulla, L. M. Kegelmeyer, Z. M. Liao, and W. Carr, "Effective and efficient optics inspection approach using machine learning algorithms," Laser-Induced Damage in Optical Materials: 2010, vol. 7842, 2010.

[18] P. Hogue and J. Coopersmith, "Development of an automated optical inspection system for determining percent area coverage for spacecraft contamination control," in Proc. of SPIE Vol, 2004, p. 157.

[19] B. Feng, F. D. Chen, B. G. Liu, and G. D. Liu, "Segmentation of Small Defects in Final Optics Damage Online Inspection Images," Proceedings of 2012 International Conference on Image Analysis and Signal Processing, pp. 110-113, 2012.

[20] A. Carr, L. Kegelmeyer, Z. Liao, G. Abdulla, D. Cross, W. Kegelmeyer, et al., "Defect classification using machine learning," in Boulder Damage Symposium XL Annual Symposium on Optical Materials for High Power Lasers, 2008, pp. 713210-713210-6.

[21] Y. Yongying, L. Chunhua, and L. Jiao, "Microscopic dark-field scattering imaging and digitalization evaluation system of defects on optical devices precision surface," *Acta Optica Sinica,* vol. 27, p. 1031, 2007.

[22] D. Sun, Y. Yang, F. Wang, L. Yang, and R. Li, "Microscopic scattering imaging system of defects on ultra-smooth surface suitable for digital image processing," in *2nd International Symposium on Advanced Optical Manufacturing and Testing Technologies*, 2006, pp. 615012-615012-6.

[23] Beis, J., Lowe, D.G. (1997). Shape indexing using approximate nearest-neighbour search in high-dimensional spaces. Proceedings of IEEE Computer Society Conference on Computer Vision and Pattern Recognition, San Juan, June 17.-19.1997.